Biophotonic probing of macromolecular transformations during apoptosis

Artem Pliss, Andrey N. Kuzmin, Aliaksandr V. Kachynski, and Paras N. Prasad[1]

Institute for Lasers, Photonics and Biophotonics, University at Buffalo, State University of New York, Buffalo, NY 14260-3000

Edited* by Peter M. Rentzepis, University of California, Irvine, CA, and approved June 8, 2010 (received for review May 10, 2010)

We introduce here multiplex nonlinear optical imaging as a powerful tool for studying the molecular organization and its transformation in cellular processes, with the specific example of apoptosis. Apoptosis is a process of self-initiated cell death, critically important for physiological regulation and elimination of genetic disorders. Nonlinear optical microscopy, combining the coherent anti-Stokes Raman scattering (CARS) microscopy and two-photon excited fluorescence (TPEF), has been used for analysis of spatial distribution of major types of biomolecules: proteins, lipids, and nucleic acids in the cells while monitoring their changes during apoptosis. CARS imaging revealed that in the nuclei of proliferating cells, the proteins are distributed nearly uniformly, with local accumulations in several nuclear structures. We have found that this distribution is abruptly disrupted at the onset of apoptosis and is transformed to a progressively irregular pattern. Fluorescence recovery after photobleaching (FRAP) studies indicate that pronounced aggregation of proteins in the nucleoplasm of apoptotic cells coincides with a gradual reduction in their mobility.

biomolecular distribution | CARS imaging | cell

Apoptosis, a highly regulated process of cell death, is an integral part of basic physiologic regulation, including tissue development and homeostasis (1), immune system operation (2), elimination of genetic disorders, and cancer prevention (3). An erroneous initiation of apoptosis in cells of neural tissue may lead to severe neurodegenerative diseases such as Alzheimer's, Huntington, and Parkinson (4). Because of the evident significance of apoptosis for the fate of an organism, considerable efforts have been dedicated to advance the understanding of this process. Along with the exploring of molecular mechanisms of initiation and regulation of apoptotic pathways, the study of the dynamics of transformations in structural organization of the apoptotic cell contributes both to the fundamentals of biology as well as to applied biomedicine (5, 6). A number of prominent morphological markers such as cytoplasmic membrane blebs, collapse of the subcellular structures, cell shrinkage, condensation, and fragmentation of the cell nucleus, etc. are routinely used for the identification of the apoptotic cells (7). However, due to the massive scale and high dynamics of structural transformations, a molecular organization of apoptotic cells has remained evasive to study by conventional biochemical and optical approaches. Traditional fluorescent methods are mostly invasive by nature, limited to visualization of the labeled molecules only and can cause severe structure artifacts and necrosis in live cells (8, 9). The understanding of molecular organization of cells and tissues can be significantly enhanced by utilizing optical vibrational spectroscopy/microscopy tools. For example, Raman spectroscopy analysis has been successfully used to detect the concentration changes of RNA, proteins, and lipids in apoptotic cells (10–12).

Coherent anti-Stokes Raman scattering (CARS), which is nonlinear Raman scattering with anti-Stokes wave detection, provides an advanced noninvasive and label-free technique capable of selective imaging of major types of macromolecules: proteins, lipids, nucleic acids, and saccharides. It involves vibrationally resonant four-wave mixing at specific molecular vibration frequencies and provides sensitivity sufficient for real-time cellular imaging comparable to that of fluorescence microscopy technique. For structural characterization of biological objects, CARS microscopy allows extracting detailed information on the major macromolecular compositions and can be used to track local biochemical changes during the apoptotic process. The first report of CARS to image the apoptotic cells utilized excitation of aliphatic C-H oscillations in the membrane lipids (13). These observations, however, did not consider contributions of other intracellular macromolecules with aliphatic C-H bonds.

At the same time, proteins, rich in aliphatic C-H bonds, are essential components of the entire cellular organization. In the cell nucleus, which is the largest organelle harboring genome and regulating essentially all cellular functions, proteins are the most abundant molecules with estimated concentration range of 100–400 mg/ml (14, 15). The dynamics and distribution of the intranuclear proteins population are among the most important factors in the structure and function organization of the cell nucleus, indispensable for understanding of the complexity of processes in apoptotic cells.

Here, we employ high resolution CARS combined with two-photon excited fluorescence (TPEF) to monitor the distribution of major types of macromolecules in live proliferating and apoptotic cells. To the best of our knowledge, this is the first study of the dynamics of macromolecular distribution throughout apoptosis. The selectivity of CARS microscopy was enhanced by utilizing synchronously generated TPEF images, using the same experimental instrumentation. CARS microscopy normally applies high intensity picosecond IR laser pulses (16), and therefore simultaneous generation of the fluorescence signal in the TPEF mode can be achieved (17) by introducing an appropriate fluorescence probe. This combined nonlinear multiplex imaging technique allows for a synchronous visualization of a variety of biomolecules, e.g., proteins and lipids by CARS, along with the molecules tagged with the fluorescence probes in TPEF mode. Because this multimodal approach combines the high specificity of fluorescence detection and ability for noninvasive visualization of entire groups of biomolecules by CARS imaging, it can provide an additional layer of information for biomedical applications.

In order to study the mobility of protein macromolecules during apoptosis, fluorescence recovery after photobleaching (FRAP) was applied. While CARS/TPEF imaging reflects the distribution of macromolecules, the FRAP measurements characterize their kinetics, providing an additional dimension of information.

This concurrent application of multiplex nonlinear optical imaging and FRAP is further enhancing the understanding of

Author contributions: A.P., A.N.K., A.V.K., and P.N.P. designed research; A.P., A.N.K., and A.V.K. performed research; A.P., A.N.K., A.V.K., and P.N.P. analyzed data; and A.P., A.N.K., A.V.K., and P.N.P. wrote the paper.

The authors declare no conflict of interest.

*This Direct Submission article had a prearranged editor.

[1]To whom correspondence should be addressed. E-mail: pnprasad@acsu.buffalo.edu.

This article contains supporting information online at www.pnas.org/lookup/suppl/doi:10.1073/pnas.1006374107/-/DCSupplemental.

molecular organization of the cell and revealing sequential transformations of the intracellular macromolecular distribution throughout the apoptotic process.

Results and Discussion

The distribution of macromolecules in the cell interior along the development of apoptosis was studied using the multiplex nonlinear optical imaging setup (see *Materials and Methods* and Fig. S1).

The vibrational bands of the aliphatic C-H bond in the frequency range 2800–3000 cm^{-1} were chosen for acquiring the CARS spectra and imaging of cells. To image proteins and lipids separately, we used the difference in the corresponding Raman/CARS bands (shown at the example of the spectra of bovine serum albumin and lipids extracted from bovine heart, where the distinct resonances for proteins at ~2930 cm^{-1} and lipids at ~2840 cm^{-1} are vividly seen) (see Fig. 1). The corresponding CARS signals in the forward direction (F-CARS) with the highest contrast between the resonant signal and the nonresonant background at the above frequencies were observed.

The CARS imaging was enhanced with the simultaneous acquisition of fluorescence signal of the specific molecules in the TPEF mode. For the monitoring of apoptotic progress, together with CARS signal of proteins and lipids, the imaging of genomic DNA and RNA was performed.

Because the DNA and RNA vibrational frequencies are barely distinguishable by the CARS approach, we stained these nucleic acids with acridine orange (3,6-Bis dimethylamino-acridine hydrochloride) and selectively visualized them in a TPEF mode in the red (RNA) and the green (DNA) fluorescent channels (18, 19). For synchronous monitoring of proteins, lipids, DNA, and RNA patterns and their correlation, CARS and TPEF imaging were performed in the same cells. This multiplex microscopy allows for a nearly simultaneous imaging of proteins, RNA, DNA, and lipids, with a short delay of ~30 sec to change to the resonance frequency from one value to another in the CARS channel.

In accordance with commonly accepted patterns (20) in the TPEF channels, the signal of genomic DNA was featuring negative staining of the nucleoli and showed minor fluctuations of the local signal intensity in the nucleoplasm. At the same time, the RNA signal, heavily accumulated in the nucleolus, reflected an intense synthesis of the ribosomal RNA and maturation of the ribosomes in this subnuclear compartment.

This experimental system allowed us also to design multiplex "hierarchical" imaging, when the specific molecules are mapped in the TPEF mode, together with the entire family of biomolecules in the CARS mode. In particular, in our study, we used this option to monitor specific protein markers of nuclear structure-function domains (SC-35, PML protein, CENPB, Nucleolin, Lamin A/C) along with the entire pool of the nuclear proteins, thus acquiring an additional layer of information on the macromolecular organization of the cell.

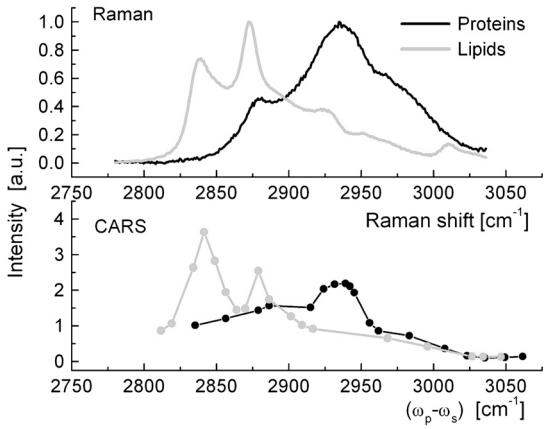

Fig. 1. Raman (upper graphs) and CARS (lower graphs) spectra of proteins and lipids derived from the bovine serum albumin (protein spectra, black) and bovine heart lipid extract (lipid spectra, gray) in the vibration frequency range 2775–3050 cm^{-1}. The distinct resonances for proteins at ~2930 cm^{-1} and lipids at ~2840 cm^{-1} are clearly seen.

In order to establish the physiological distribution of macromolecules, we performed high resolution multiplex nonlinear CARS/TPEF imaging throughout the interphase of the cell cycle as well as during the execution of apoptosis.

Based on analysis of several hundred cells, our data were very reproducible. During the imaging live cells were maintained at the physiological conditions as described in *Materials and Methods*. Representative distributions of the major groups of macromolecules—proteins and lipids in the CARS mode along with RNA and DNA in the TPEF mode in both the exponentially growing and the apoptotic cells—are presented in Fig. 2 and Fig. S2.

A detailed analysis of the acquired images expands the canonic views on the structural organization of the cell nucleus and traces the progressive transformations in the distributions of macromolecules in the process of apoptosis.

In the nuclei of exponentially growing cells, we have observed that the signal from proteins was accumulated in the nucleolus and the nuclear lamina (Fig. 2*A* and Fig. 3) as it was confirmed by an overlap with nucleolin and lamin A/C staining performed in fixed cells. At the same time, to our surprise, we observed only minor variations in the proteins' signal intensity in the rest of the nuclear volume, including many prominent subnuclear domains, as is shown in Fig. 3. For instance, in the nuclear speckles, which serve as the hubs for RNA processing and certain proteins' modifications and locally accumulate numerous protein-based enzymes (21–23), we observed only minor fluctuation in the proteins' signal intensity (Fig. 3). Similar uniform distribution of proteins was also observed in the clusters of heterochromatin, and the PML bodies.

We thus conclude that, despite a remarkable heterogeneity in the molecular content of the subnuclear domains (21, 24, 25), the overall concentration of protein molecules is relatively uniform in substantial part of the nuclear volume (Fig. 3).

For the interpretation of our results, a concept of self-organization of the cell nuclear structure (14, 26) can be applied. This model, based on fluorescent visualization of specific nuclear factors (26, 27), assumes that many macromolecules are distributed in the nuclear volume via the nearly stochastic motion, which facilitates their productive interactions and provides a basis for the dynamic formation of subnuclear structure-function domains (15, 26). Consistently, a quasi-uniform distribution of proteins in the cell nuclear volume revealed by our CARS imaging, (Figs. 2 and 3 and Fig. S3) is caused, apparently, by fast circulation of protein molecules, including constituents of many subnuclear domains via homogeneous, most probably thermal, diffusion, which results into overall concentration balance under the thermodynamic equilibrium conditions.

In the cytoplasm, as it is shown in Fig. 2 and Fig. S2, the CARS signal reveals accumulation of proteins into mildly polarized cytoskeleton fibers. The CARS signal of lipids is dominant in the cytoplasmic membrane and the nuclear envelope (Fig. S2). Often cytoplasmic inclusions in the form of lipid droplets were seen.

Previously, by the immunocytochemical approaches, it has been shown that during the apoptosis the nuclear structure-function domains collapse, agglomerations of macromolecules at the advanced stages of apoptosis may form de novo, chromatin transforms to compact chromatin bodies, and the entire nucleus shrinks (28–30). The scale and dynamics of macromolecular transformation can further be comprehensively assessed by

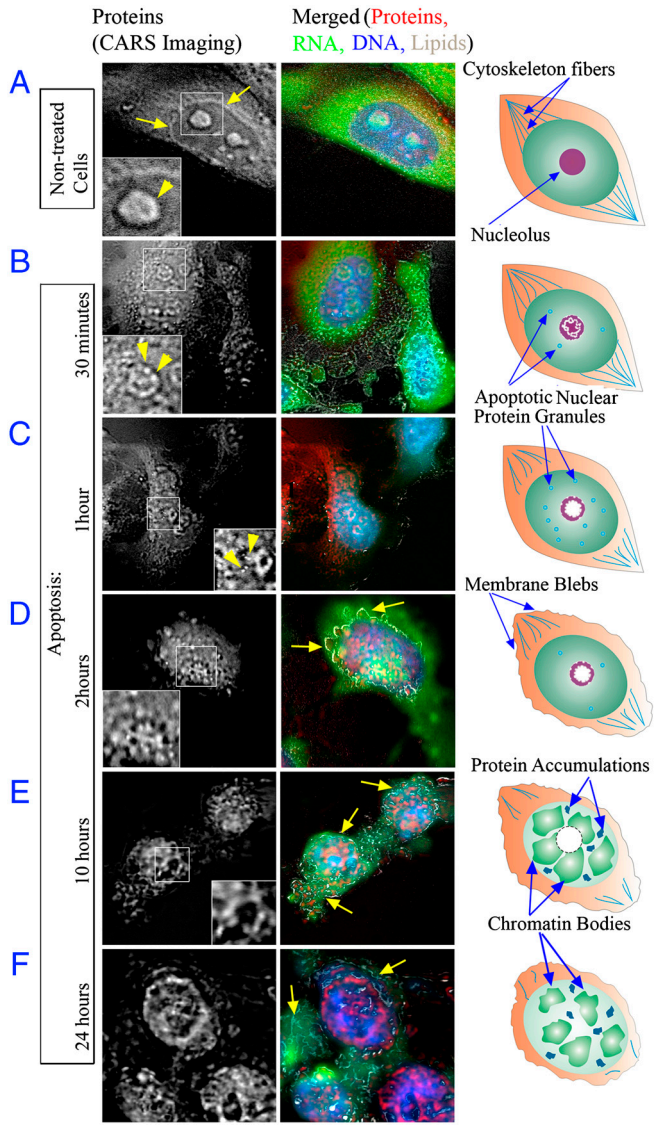

Fig. 2. The distribution of proteins, lipids, DNA, and RNA in dividing and apoptotic HeLa cells visualized by multimodal CARS/TPEF imaging. During the imaging live cells were maintained at the physiological conditions. Proteins and lipids were observed in the CARS mode at their characteristic vibrations of 2930 cm^{-1} and 2840 cm^{-1}, respectively. Nucleic acids, stained by acridine orange, were acquired in the red (RNA) and green (DNA) fluorescence channels in TPEF mode. In the right panels, schematics of the macromolecular organization of cells are represented. The CARS signal from proteins is represented in the left panels. The panels in the middle represent merger signals of the proteins (red), RNA (green), DNA (blue), and lipids (gray). The white-outlined areas in the protein channel are enlarged below. (*A*) Nontreated cells. The signal from proteins is accumulated in the nucleolus (*Inset*, arrowhead) and the nuclear lamina (arrows). In the rest of the nuclear volume, the intensity of the protein signal is nearly uniform. (*B–F*) Representative cells at the subsequent stages of the apoptotic development. (*B*) 30 minutes following the initiation of apoptosis, the distribution of proteins is altered in the nucleolus (*Inset*, arrowheads) and the novel structure, apoptotic nuclear protein granules (ANPG), emerged in the nucleoplasm. In the cytoplasm, cytoskeleton fibers begin to lose their structural polarization. (*C*) The pattern of proteins becomes increasingly irregular, and ANPG become prominent (*Inset*, arrowheads). (*D*) The nucleolar proteins are forming a complex meshwork (*Inset*). The apoptotic membrane blebs are seen (*D* and *E* merged panels, arrows), ANPG disintegrate. (*E* and *F*) Proteins abandon the nucleolus and demonstrate a highly irregular distribution in the nucleoplasm; the genomic DNA is condensing to chromatin bodies and partially segregates from the proteins.

CARS imaging, uniquely enabling noninvasive data collection during the entire process of apoptosis.

To study the molecular distribution in the apoptotic cells, the apoptosis was initiated (31) and a progressive reorganization of the cell nucleus was followed. The early stages of apoptosis were identified by the RNA distribution pattern. In 30 minutes after initiation of apoptosis, we observed that RNA staining persisted only at the nucleolar periphery (Fig. 2*B* and Fig. S2*B*), while in the nucleolar interior, where the rRNA synthetic/processing machinery is accumulated (32), only a weak RNA signal was seen (Fig. 2). This transformation of nucleolus is due to suppression of the ribosomal RNA synthesis and is one of the earliest hallmarks in the apoptotic development (33).

The protein's CARS signal reveals a striking reorganization of the nucleoli at this early stage of apoptosis (Fig. 2*B*). The protein molecules were accumulated in globules at the periphery of the nucleolus (Fig. 2*B Inset*). In the nucleolar interior, we observed a significant decrease in the signal intensity (Fig. 2*B*); the remaining nucleolar proteins dramatically changed their distribution to a progressively forming globular meshwork (Fig. 2*D*, *Inset*). At a more advanced stage of apoptotic progression (~5 hours and longer), proteins almost completely abandoned the nucleolus. In the late apoptotic cells, the residual nucleoli appeared as mostly hollow domains, depleted of proteins and with diffuse RNA staining (Fig. 2*E*). Finally, the nucleoli completely disintegrated following ~24 hours of apoptotic development (Fig. 2*F*).

In the nucleoplasm outside of the nucleolus, as shown in Fig. 2, we observed a pronounced redistribution of proteins to a less uniform pattern. In the nuclei of early apoptotic cells, proteins formed focal accumulations of ~0.5 μm in diameter, designated here as "apoptotic nuclear protein granules" (ANPG). These ANPG are hallmarks of early stages of apoptosis and appear in the nucleoplasm following ~30 minutes after the initiation of this process. The number of ANPG reached a maximum at approximately 1 h of the apoptotic process when, on the average, 15–20 bright foci per cell nucleus were regularly seen (Fig. 2*C Inset*, arrowheads and Fig. S3). Then, 90–120 min following the apoptotic initiation, ANPG became less intense and less numerous and, finally, could not be distinguished anymore from the background of nuclear proteins (Fig. 2 *D–F*).

Further transformations during apoptosis led to a progressive aggregation of proteins. Just several hours after the apoptotic initiation, the cell nuclei exhibited protein accumulations in clusters of several tens of cubic microns, as demonstrated by signifi-

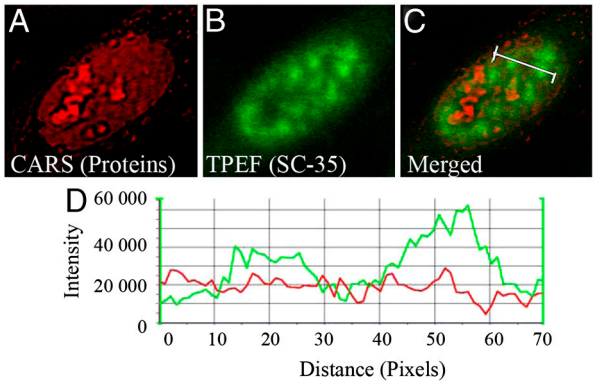

Fig. 3. Simultaneous visualization of the bulk nuclear proteins in CARS mode and specific protein epitopes (SC-35) in the TPEF mode. Imaging was performed in the fixed cells. (*A*) Proteins were visualized at characteristic vibration of 2930 cm^{-1} in the CARS mode. (*B*) Marker of the nuclear speckles, SC-35 was labeled with fluorochrome-conjugated antibodies and visualized in the TPEF mode simultaneously with the proteins CARS signal. (*C*) A merged image of *A* and *B*. (*D*) An intensity line profile of SC- 35 (green line) and proteins CARS signal (red line) drawn through *C*. The intensity of CARS signal is relatively uniform in the nuclear speckles and in the surrounding nucleoplasm.

cant fluctuations of the signal intensity (Fig. S3). Furthermore, at the late stages of apoptosis, when the nuclear chromatin is being clustered to dense chromatin bodies, we observed a partial segregation of DNA and proteins, with multiple protein accumulations in gaps between the chromatin bodies (Fig. 2 *E* and *F*).

Thus, the CARS microscopy data presented in Fig. 2 and Fig. S3 demonstrate that apoptosis development is accompanied by a pronounced aggregation of nuclear proteins throughout the cell nucleus. Such protein aggregation can be caused by numerous factors in the apoptotic development, such as caspase mediated proteolytic cleavage (34), collapse of the subnuclear compartments (35, 36), random interaction of damaged macromolecules, etc. Furthermore, a progressive emergence of protein aggregates is indicative of trapping of nuclear macromolecular complexes, which can interfere with their mobility.

To support the interpretation of CARS imaging results by measuring the proteins' intranuclear mobility during the apoptosis, the FRAP experiments (37) on the cells transfected with green fluorescent protein (GFP) were carried out. The FRAP experiments were performed at random spot-bleached sites in the nucleoplasm of either nontreated or apoptotic cells (Fig. 4*A*); over 50 cells in total were analyzed. Because no specific interactions of nuclear constituents and GFP are expected, we utilized the fluorescence recovery rate for the evaluation of overall diffusion kinetics of native nuclear proteins along the execution of apoptosis. The averaged FRAP results point to a progressive slowdown in fluorescence recovery as the apoptosis develops (Fig. 4*B*). In the nonapoptotic cells, the fluorescence half-recovery time varied from 0.18 to 0.5 sec, whereas in cells at second, fourth, and 24th hours following apoptosis initiation, this parameter was ranging from 0.42 to 0.92 sec, from 0.5 to 2.65 sec, and from 0.58 to 7 sec, respectively (Fig. 4). We have further observed that at more advanced stages of apoptotic development the GFP in the cell nucleus became virtually immobile (Fig. S4). Thus, we measured a steady decrease in the average GFP mobility as apoptosis progressed. The variability in GFP mobility observed in the different cells was caused, apparently, by asynchrony in the development of apoptosis.

CARS/TPEF imaging and FRAP measurements were performed using the same protocol for apoptosis induction and analyzed over a significant number of experiments in order to find correlation and to generalize data obtained by these techniques. The CARS microscopy data and the FRAP measurement together demonstrate that the major transformations of the nuclear structure seen in apoptotic cells may correlate with a reduction in the diffusion rate of macromolecular complexes in the cell nuclei. A correlation of the data obtained in CARS and FRAP experiments emphasizes the importance of stochastic molecular motions for the formation and maintenance of nuclear structure.

In summary, our data, based on combined applications of multimodal CARS/TPEF nonlinear optical imaging, together with FRAP study, allowed us to monitor the macromolecular compositions of the cellular interior and their characteristic specific transformations during apoptosis. Our results provide previously undescribed details on the formation of apoptosis

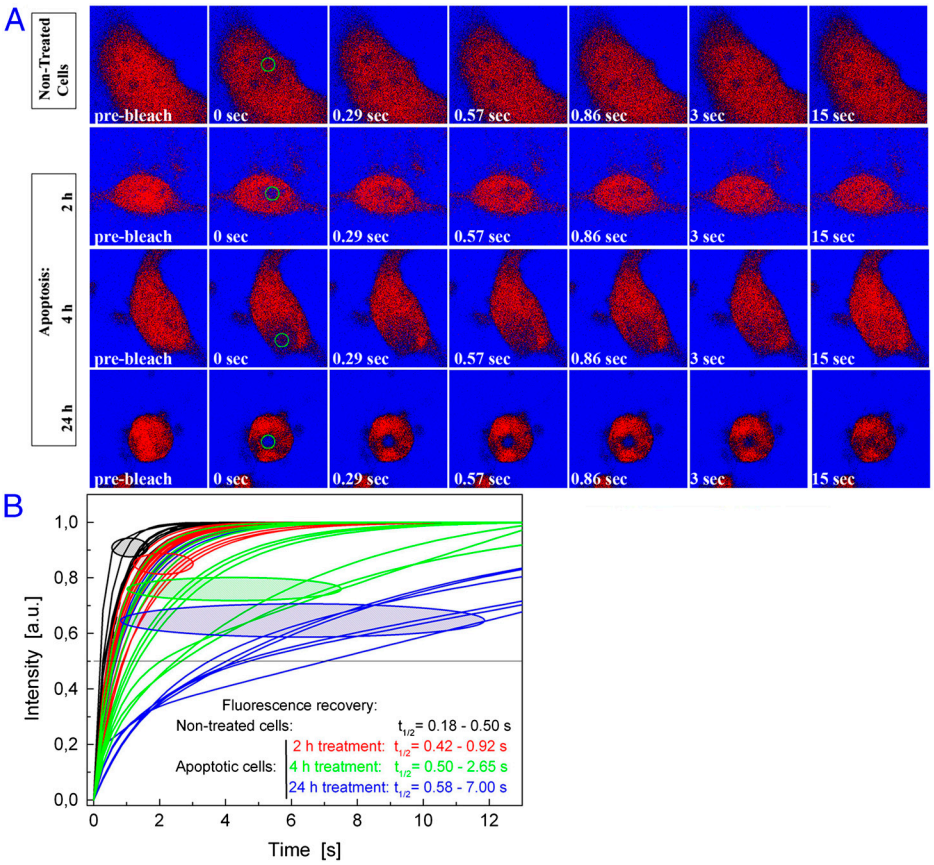

Fig. 4. FRAP studies of the GFP diffusion rate in the dividing and apoptotic cells. (*A*) FRAP experiments were performed at the physiological conditions in the exponentially growing and apoptotic cells (top to bottom nontreated cells and at second, fourth, and 24th hours of apoptotic development, as indicated), images are pseudocolored. The green circle indicates a photobleached spot. Apoptotic cells demonstrate progressive slowdown in the recovery of the fluorescence. (*B*) FRAP data for each experimental group of cells is represented as color-coded curves. Due to the high variability in the GFP recovery rate at advanced stages of apoptosis the data are nor averaged and presented as measurements into individual cells. The range of half-time of fluorescence recovery ($t_{1/2}$) in each experimental group is shown and vividly represented by the dashed ellipses areas. The data indicate a gradual increase in the $t_{1/2}$ along the development of apoptosis.

hallmarks and clearly contribute to an understanding of correlation between the macromolecular distribution and the physiological condition of the cell.

Materials and Methods

Cell Culture, Fluorescent Staining, and Induction of Apoptosis. HeLa cells were grown in glass-bottom dishes (Mattek) and cultured in Advanced DMEM (Invitrogen), supplemented with 2.5% fetal calf serum (Sigma) at 37 °C in a humidified atmosphere containing 5% CO_2. To stain nucleic acids, the cells were incubated for 20 min with 5 μM acridine orange. For the immunolabeling, cells were fixed 12 min in 4% PFA/PBS and permeabilized 5 min in 0.25% Triton X-100. The following antibodies were used: mouse anti-SC35 and antilamin A/C antibodies, rabbit anti-Centromeric Protein B, antinucleolin and anti-PML antibodies (Abcam). The secondary antirabbit and antimouse antibodies were conjugated with Alexa 488 (Invitrogen). Apoptosis was induced by incubation with 1.5 μM Staurosporine, the apoptotic initiation and viability of cells were monitored by annexin V-Cy3/Sytox Green apoptotic detection kit (Abcam). The above protocol (31) produces apoptosis in nearly 100% of cells. In CARS/TPEF live cells experiments, the cells were maintained at 37 °C and 5% CO_2 in a Live-Cell incubator (Pathology Devices) mounted at the microscope stage. In the FRAP studies these physiological conditions were maintained by micro-environmental system from Warner Instrument Co.

CARS-TPEF Setup. A simplified schematic for the CARS setup (38, 39) is shown in Fig. S1. A picosecond Nd : YVO_4 (picoTRAIN IC-10000, HighQ Laser) with pulse width ~6 ps and a repetition rate of 76 MHz was used as the source of the Stokes wave at ω_s (1064 nm) and for synchronous pump (532 nm) of tunable (680–980 nm) optical parametric oscillator (OPO, Levante, APE) with an output pulse width of ~6 ps. The synchronously pumped OPO serves as a source of the pump/probe wave at $\omega_p = \omega_{\text{pump}} = \omega_{\text{probe}}$. The two picosecond laser beams are made coincident in time and space using a series of dichroic mirrors and line delay and focused onto the sample using a $60\times$ NA $= 1.3$ Olympus objective lens. The configuration of our experimental setup enables the CARS imaging with the vibration frequencies in the spectral range of 900–3000 cm^{-1}. Six detection channels—two forward and four backward—allowed us to record of forward- and backward-propagated CARS and fluorescence signals. The set of dichroic mirrors (M) and a series of barrier filters (F) are used for spectral selection of signals for registration. An XY scanner (GSI Lumonics), a Z stage (Piezosystem Jena), and the detection system (Solar TII) allow for acquisition of 1 frame per second in four channels at the same laser scan or series of scans. We characterized the space resolution of CARS system at ~200 nm in lateral plane and ~500 nm in Z plane by imaging polystyrene beads with calibrated diameters. Imaging of lipids and proteins was performed at 2840 cm^{-1} and 2930 cm^{-1} respectively. Both frequency shifts and their position at the vibration spectrum (Fig. 1) were chosen to receive the images of the specific macromolecules with the highest contrast to others constituents in their highly mixed conditions (for example, vibration frequency adjustment to 2840 cm^{-1} and 2930 cm^{-1} results in the highest ratio of the lipid's signal to the protein's, Fig. 1). Close proximity between CARS signal peaks allows for fast tune the pump (OPO) wavelength providing minimum time delay between image scans corresponding to the proteins and lipids. All the acquired CARS images were released from nonresonance background by applying the standard procedure of the digital images processing at the resonance and out of resonance vibration frequencies. In the similar manner lipids' images generated at 2840 cm^{-1} were released from residual signal of proteins by digital images subtraction. Such digital image processing is applicable in case if no noticeable morphology changes or cell motion between images scans at two different vibration frequencies are expected. In our experiments delay between sequential scans was in a range of several seconds, and we did not observe any inadmissible cell motion or distortion. For Raman spectrometry we used custom made Raman microspectrometer based on the inverted Nikon TE200 microscope, He-Ne laser (Coherent, 632.8 nm) for excitation, fiber-input MS3501i imaging monochromator/spectrograph (Solar TII), and Proscan SI HS 101H CCD camera.

FRAP Data Analysis. FRAP analysis was performed using the Leica SP2 confocal laser scanning microscope and the 488-nm Ar laser as described previously (40). Cells with representative morphology expressing moderate levels of GFP were randomly selected for the FRAP measurements. FRAP images were acquired every ~0.25 s for 15–30 sec using a 63×1.4 NA oil immersion objective. The FRAP data were obtained from the FRAP module of standard Leica SP2 software installed on a microscope setup. Recovery measurements were quantified by fitting normalized fluorescence intensities of the bleached areas to the prebleached signal intensity. The range of $t_{1/2}$ value is each experimental group of cells is shown on a graph and represented by the dashed areas.

ACKNOWLEDGMENTS. The authors are grateful to Drs. Kenneth M. Tramposch, Earl J Bergey, and Tymish Ohulchanskyy for extensive discussions. These studies were supported by a grant from the John R. Oishei Foundation.

1. Jacobson MD, Weil M, and Raff MC (1997) Programmed cell death in animal development. *Cell* 88:347–354.
2. Opferman JT, Korsmeyer SJ (2003) Apoptosis in the development and maintenance of the immune system. *Nat Immunol* 4:410–415.
3. Cotter TG (2009) Apoptosis and cancer: The genesis of a research field. *Nat Rev Cancer* 9:501–507.
4. Kermer P, Liman J, Weishaupt JH, Bahr M (2004) Neuronal apoptosis in neurodegenerative diseases: From basic research to clinical application. *Neurodegener Dis* 1:9–19.
5. Blankenberg FG, Tait JF, Strauss HW (2000) Apoptotic cell death: Its implications for imaging in the next millennium. *Eur J Nucl Med* 27:359–367.
6. Weissleder RandPittet MJ (2008) Imaging in the era of molecular oncology. *Nature* 452:580–589.
7. Galluzzi L, et al. (2007) Cell death modalities: Classification and pathophysiological implications. *Cell Death Differ* 14:1237–1243.
8. Stephens DJ, Allan VJ (2003) Light microscopy techniques for live cell imaging. *Science* 300:82–86.
9. Frigault MM, Lacoste J, Swift JL, Brown CM (2009) Live-cell microscopy—Tips and tools. *J Cell Sci* 122:753–767.
10. Krafft C, Knetschke T, Funk RH, Salzer R (2006) Studies on stress-induced changes at the subcellular level by Raman microspectroscopic mapping. *Anal Chem* 78:4424–4429.
11. Swain RJ, Stevens MM (2007) Raman microspectroscopy for non-invasive biochemical analysis of single cells. *Biochem Soc Trans* 35:544–549.
12. Uzunbajakava N, et al. (2003) Nonresonant confocal Raman imaging of DNA and protein distribution in apoptotic cells. *Biophys J* 84:3968–3981.
13. Cheng JX, Jia YK, Zheng GF, Xie XS (2002) Laser-scanning coherent anti-stokes Raman scattering microscopy and applications to cell biology. *Biophy J* 83:502–509.
14. Misteli T (2007) Beyond the sequence: Cellular organization of genome function. *Cell* 128:787–800.
15. Hancock R (2004) A role for macromolecular crowding effects in the assembly and function of compartments in the nucleus. *J Struct Biol* 146:281–290.
16. Volkmer A (2005) Vibrational imaging and microspectroscopies based on coherent anti-Stokes Raman scattering microscopy. *J Phys D Appl Phys* 38:R59–R81.
17. Evans CL, et al. (2005) Chemical imaging of tissue in vivo with video-rate coherent anti-Stokes Raman scattering microscopy. *Proc Natl Acad Sci USA* 102:16807–16812.
18. Prasad PN (2003) *Introduction to biophotonics* (Wiley-Interscience, Hoboken, NJ), xvii, 593, [598] of plates.
19. Kornfield HJ, Werder AA (1960) A differential nucleic acid fluorescent stain applied to cell culture systems. *Cancer* 13:458–461.
20. Martin RM, Leonhardt H, and Cardoso MC (2005) DNA labeling in living cells. *Cytometry A* 67:45–52.
21. Lamond AI, Spector DL (2003) Nuclear speckles: A model for nuclear organelles. *Nat Rev Mol Cell Biol* 4:605–612.
22. Maul GG, Negorev D, Bell P, Ishov AM (2000) Review: Properties and assembly mechanisms of ND10, PML bodies, or PODs. *J Struct Biol* 129:278–287.
23. Bernardi R, Pandolfi PP (2007) Structure, dynamics and functions of promyelocytic leukaemia nuclear bodies. *Nat Rev Mol Cell Biol* 8:1006–1016.
24. Spector DL (1993) Macromolecular domains within the cell nucleus. *Annu Rev Cell Biol* 9:265–315.
25. Fraser P, Bickmore W (2007) Nuclear organization of the genome and the potential for gene regulation. *Nature* 447:413–417.
26. Misteli T (2008) Cell biology: Nuclear order out of chaos. *Nature* 456:333–334.
27. Phair RD, et al. (2004) Global nature of dynamic protein-chromatin interactions in vivo: Three-dimensional genome scanning and dynamic interaction networks of chromatin proteins. *Mol Cell Biol* 24:6393–6402.
28. Ziegler U, Groscurth P (2004) Morphological features of cell death. *News Physiol Sci* 19:124–128.
29. Scovassi AI, Bottone MG, Biggiogera M, Pellicciari C (2008) Dynamic relocation of nuclear proteins during the execution phase of apoptosis. *Biochem Pharmacol* 76:1440–1450.
30. Taylor RC, Cullen SP, Martin SJ (2008) Apoptosis: Controlled demolition at the cellular level. *Nat Rev Mol Cell Biol* 9:231–241.
31. Bertrand R, Solary E, O'Connor P, Kohn KW, Pommier Y (1994) Induction of a common pathway of apoptosis by staurosporine. *Exp Cell Res* 211:314–321.
32. Koberna K, et al. (2002) Ribosomal genes in focus: New transcripts label the dense fibrillar components and form clusters indicative of "Christmas trees" in situ. *J Cell Biol* 157:743–748.
33. Martelli AM, et al. (2000) Behavior of nucleolar proteins during the course of apoptosis in camptothecin-treated HL60 cells. *J Cell Biochem* 78:264–277.
34. Kumar S (2007) Caspase function in programmed cell death. *Cell Death Differ* 14:32–43.
35. Biggiogera M, et al. (2004) Rearrangement of nuclear ribonucleoprotein (RNP)-containing structures during apoptosis and transcriptional arrest. *Biol Cell* 96:603–615.

36. Robertson JD, Orrenius S, and Zhivotovsky B (2000) Review: Nuclear events in apoptosis. *J Struct Biol* 129:346–358.
37. Phair RD, Misteli T (2000) High mobility of proteins in the mammalian cell nucleus. *Nature* 404:604–609.
38. Kachynski AV, Kuzmin AN, Prasad PN, Smalyukh II (2007) Coherent anti-Stokes Raman scattering polarized microscopy of three-dimensional director structures in liquid crystals. *Appl Phys Lett* 91:151905.
39. Kachynski AV, Kuzmin AN, Prasad PN, and Smalyukh II (2008) Realignment-enhanced coherent anti-Stokes Raman scattering and three-dimensional imaging in anisotropic fluids. *Opt Express* 16:10617–10632.
40. Dunham-Ems SM, et al. (2009) Fibroblast growth factor receptor-1 (FGFR1) nuclear dynamics reveal a novel mechanism in transcription control. *Mol Biol Cell* 20:2401–2412.